Supplementary Information

An unusual zinc substrate-induced self-construction route to various hierarchical architectures of hydrated tungsten oxide

De-Kun Ma,*[a] Jing-Lu Jiang,[a] Jia-Rui Huang,[b] Dong-Peng Yang,[a] Ping Cai[a] Li-Jie Zhang[a] and Shao-Ming Huang*[a]

[a] *Nanomaterials and Chemistry Key Laboratory, Wenzhou University, Wenzhou, Zhejiang 325027, P. R. China. Fax: (+86)-577-88373064; Tel: (+86)-577-88373031; E-mail: dkma@wzu.edu.cn; smhuang@wzu.edu.cn*
[b] *College of Chemistry and Materials Science, Anhui Normal University, Wuhu, Anhui 241000, P. R. China. E-mail: jrhuang@mail.ahnu.edu.cn*

Experimental Section

***Material Synthesis*:** In a typical synthesis, a piece of zinc foil (thickness: 0.25 mm, length: 10 mm, width: 6 mm, used after rinsing with diluted hydrochloric acid, distilled water, and ethanol, respectively), 2 mmol of $Na_2WO_4 \cdot 2H_2O$, and 40 mL of distilled water were placed in a stainless steel autoclave with a Teflon liner of 60 mL capacity. Then the pH value of the aqueous solution was adjusted to 2.7 using HNO_3 (1 $mol \cdot L^{-1}$). After that, the autoclave was sealed and heated at 180 ^oC for different period of time and then cooled in air to room temperature. The zinc foil was taken out of the solution, washed with ethanol, and finally air-dried for characterization.

***Photocatalytic properties study*:** photocatalytic activities of various hierarchical architectures were evaluated by degradation of RhB under 300W Xe lamp (purchased from Nanjing Sidongke electric equipment Co. Ltd., P.R. China) irradiation. In every experiment, a zinc substrate contained photocatalysts was added to 100 mL of RhB solution (10^{-5} mol/L). Before illumination, the solution was magnetically stirred in the dark for 12 h to ensure the establishment of an adsorption-desorption equilibrium between the photocatalysts and RhB. After that, the solution was exposed to Xe lamp light irradiation under magnetic stirring. At given time intervals, 3 mL aliquots were sampled and centrifuged to remove the photocatalyst particles. Then, the filtrates were analyzed by recording variations of the absorption band maximum (553 nm) in the UV-vis spectra of RhB by using a Shimadzu UV2501PC spectrophotometer.

***Gas sensor fabrication and response test*:** the as-prepared $WO_3 \cdot 0.33H_2O$ double-layer nanorods arrays architectures were directly coated on the outer surface of an alumina tube-like substrate on which a pair of Au electrodes had been printed previously, followed by drying at 60 ^oC for about 2 h and subsequent annealing at 450 ^oC for about 3 h. Finally, a small Ni-Cr alloy coil was inserted into the tube as a heater, which provided the working temperature of the gas sensor. The gas sensor fabricated with a double-layer nanorods arrays film on a ceramic tube is shown in Figure S1a. In order to improve the long-term stability, the sensors were kept at the working temperature for several days. A stationary state gas distribution method was used for testing gas response in dry air. In the measurement of electric circuit for gas sensors (Figure S1b), a load resistor was connected in series with a gas sensor. The circuit voltage was set at 5 V, and the output voltage (V_{out}) was the terminal voltage of the load resistor. The working temperature of a sensor was adjusted through varying the heating voltage. The resistance of a sensor in air or test gas was measured by monitoring V_{out}. The test was operated in a measuring system of ART-2000A (Art Beijing Science and Technology Development Co. Ltd., P.R. China). Detecting gases, C_2H_5OH, were injected into a test chamber and mixed with air. The gas response of the sensor in this paper was defined as $S = R_a/R_g$ (reducing gases), where R_a and R_g were the resistance in air and test gas, respectively. The response or recovery time was expressed as the time taken for the sensor output to reach 90% of its saturation after applying or switching off the gas in a step function.

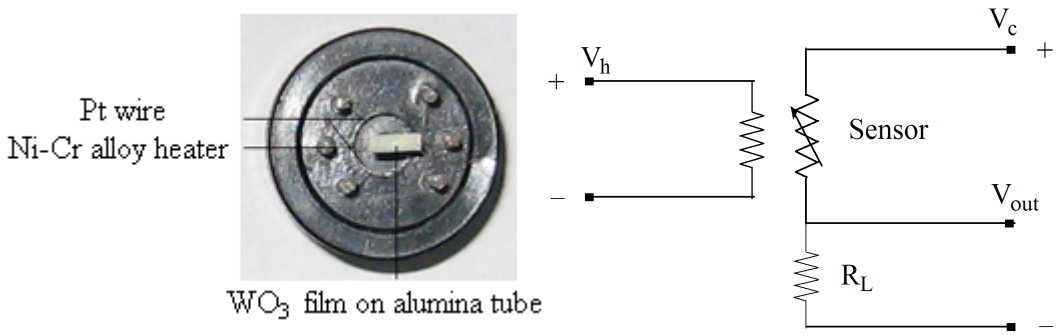

Fig. S1. (a) Photo of the gas sensor fabricated with a double-layer nanorods arrays film on a ceramic tube. (b) The electric circuit for the gas sensor.

***Material Characterizations*:** Powder X-ray diffraction (XRD) was carried out with a Bruker D8 Advance X-ray diffractometer using Cu Kα radiation (λ = 0.15418 nm) at a scanning rate of 8^{o}/min in the 2θ range from 10 to 70^{o}. Field emission scanning electron microscopy (FE-SEM) images and energy-dispersive X-ray (EDX) spectroscopy were taken on a Nova NanoSEM 200 scanning electron microscope (FEI Inc.).

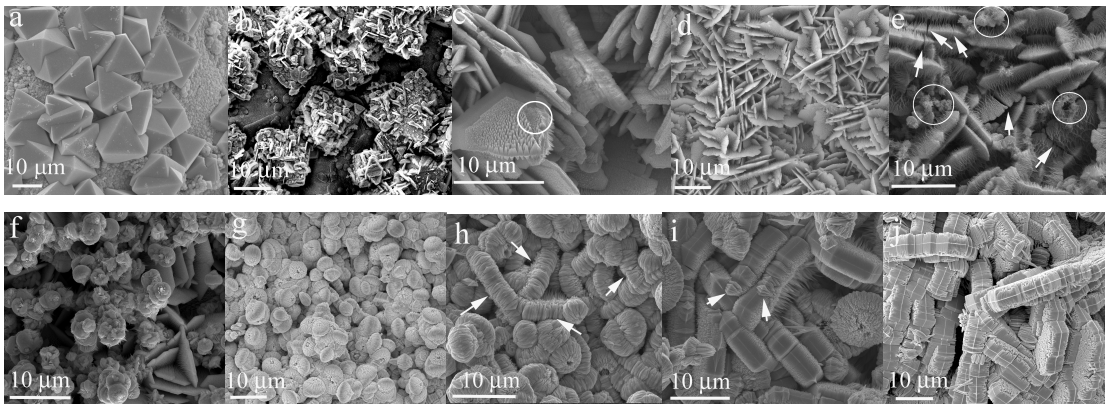

Fig. S2. FE-SEM images of the samples hydrothermally grown on zinc substrate for different reaction periods. (a) For 1.5 h, the products are octahedron-shaped aggregates. (b) For 2 h, these octahedrons with smooth surfaces began to exfoliate to form small pieces with triangular hierarchical nanowires arrays. (c) For 3 h, these nanowires arrays would develop into larger flakes. The white circular frame areas show the evolution trail from nanowires arrays to flakes. (d) For 4 h, these hierarchical triangular nanowires arrays completely developed into larger flakes superstructures. (e) For 7 h, some flakes superstructures were ruptured (see the place where the white arrowheads point) and broken parts self-assembled into small lantern-like microspheres (see the white circular frame areas). (f) For 8 h, more and more lantern-like microspheres formed. (g) For 10 h, flakes superstructures disappeared and transformed into lantern-like hierarchical microspheres completely. (h) For 11 h, these lantern-like microspheres were unwrapped and restructured. The white arrowheads indicate several typical unwrapped and restructured lantern-like microspheres. (i) For 12 h, more double-layer nanorods arrays were obtained. The arrowheads show the evolution trail from unwrapped lanterns to double-layer nanorods arrays. (j) For 14 h, lantern-like superstructures were wholly transformed into double-layer nanorods arrays. To understand the reasons why octahedron exfoliate along {111} planes, we start from the crystal structure of $WO_3 \cdot 0.5\ H_2O$. As the projection of the crystal structure along (111) plane normal direction shows, water molecules range close along this direction. Therefore, during synthesis process, water molecules were easy to dehydrate and exfoliated along (111) planes of $WO_3 \cdot 0.5\ H_2O$ at high hydrothermal temperature.

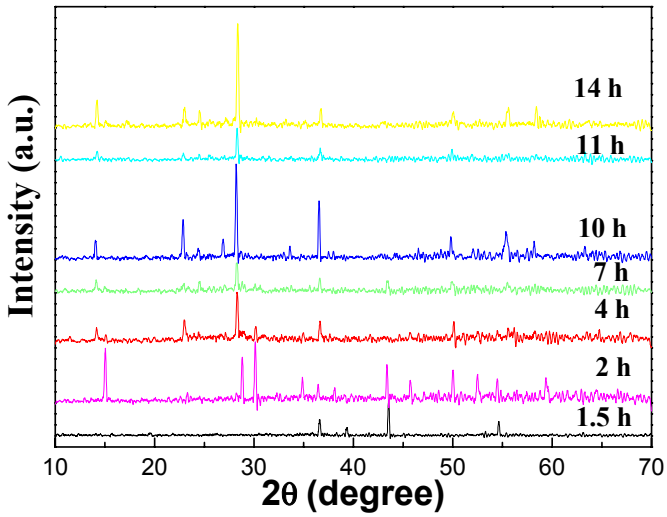

Fig. S3. XRD patterns of the samples for different reaction time periods. For 1.5 h, no diffraction peaks from the products were detected except zinc from substrate. For 2 h, the reflection peaks of the products can be indexed to predominant cubic phase of $WO_3 \cdot 0.5H_2O$ (JCPDS Card No. 44-0363) and a spot of hexagonal phase of $WO_3 \cdot 0.33H_2O$ (JCPDS Card No. 35-1001). For 4 h, the products can be indexed to a small quantity of cubic phase of $WO_3 \cdot 0.5H_2O$ and predominant hexagonal phase of $WO_3 \cdot 0.33H_2O$. For 7-14 h, the products are pure $WO_3 \cdot 0.33H_2O$. The diffraction peak intensity of the products from 4 to 14 h went through a fall — rise — fall — rise process.

Formation process of various hierarchical architectures:

According to the XRD and SEM investigations shown above, the formation process of various morphologies can be depicted as follows. (1) Primary $WO_3 \cdot nH_2O$ octahedron precursors were formed initially because of the inducing effect of active zinc substrate under the synthetic condition. (2) These newborn octahedron began to exfoliate along (111}) planes and grew into nanowires arrays because of anisotropy of crystal structure of $WO_3 \cdot 0.5\ H_2O$. To understand the reasons why octahedron exfoliate along (111) planes, we start from the crystal structure of $WO_3 \cdot 0.5\ H_2O$. As the projection of the crystal structure along (111) plane normal direction shows, water molecules range close along this direction. Therefore, during synthesis process, water molecules were easy to dehydrate and exfoliated along (111) planes of $WO_3 \cdot 0.5\ H_2O$ at high hydrothermal temperature. (3) The octahedral frames collapsed completely. Nanowires arrays broke down and grew into interlaced petal-like superstructures of $WO_3 \cdot 0.33H_2O$. (4) Further hydrothermal growth, flakes superstructures were ruptured. The projection of the crystal structure of $WO_3 \cdot 0.33\ H_2O$ along (001) plane normal direction shows water molecules range close in *ab* plane. Therefore, water molecules were easy to dehydrate along *ab* plane. In other words, *ab* plane of $WO_3 \cdot 0.33\ H_2O$ easily dissociated and thus the rupture of flakes superstructures were observed. (5) Ruptured parts would recombine into lantern-like architectures because this kind of structure owned relative small surface energy. (6) When reaction time was further prolonged, lantern-like architectures was unwrapped and assembled into larger double-layer nanorods arrays in order to further decrease systematic energy. Thus it could be seen that the whole morphological evolution from hierarchical octahedron, through flake to lantern-like structures, then to the final double-layer nanorods arrays went through a sequential self-construction process.

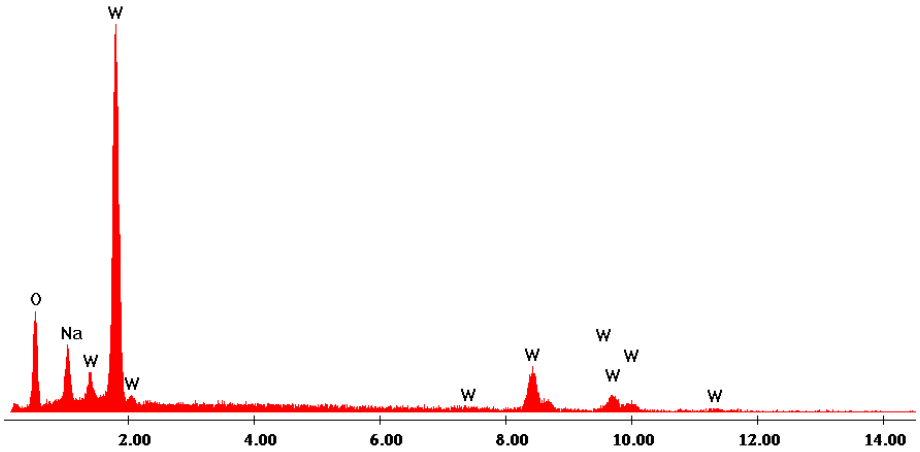

Fig. S4. EDX spectrum of the sample hydrothermally synthesized at 180 ^{o}C for 1.5 h.

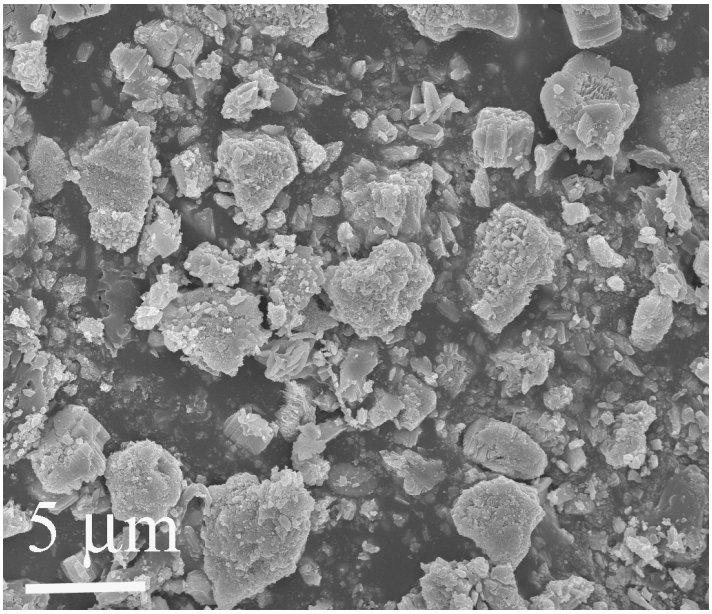

Fig. S5. FE-SEM image of the sample synthesized by replacing zinc substrate with zinc powder.

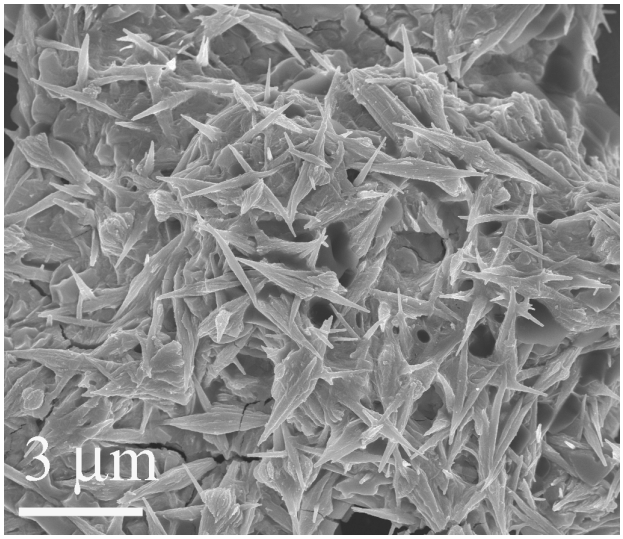

Fig. S6. FE-SEM image of the sample obtained on the inert silicon oxide substrate for 2 h.